Matildite *versus* Schapbachite: First-Principles Investigation on $AgBiS_2$ Photoactivity Origin

Francesc Viñes,[1] María Bernechea,[2,3] Gerasimos Konstantatos,[2,4] and Francesc Illas[1,*]

[1] *Departament de Ciència de Materials i Química Física & Institut de Química Teòrica i Computacional (IQTCUB), Universitat de Barcelona, C/Martí i Franquès 1, 08028 Barcelona, Spain.*

[2] *ICFO-Institut de Ciències Fotòniques. The Barcelona Institute of Science and Technology, 08860 Castelldefels (Barcelona), Spain.*

[3] *Cardiff School of Engineering, Cardiff University, Cardiff CF24 3AA, Wales, UK.*

[3 4] *ICREA-Institució Catalana de Recerca i Estudis Avançats. Passeig Lluís Companys 23, 08010 Barcelona, Spain.*

* francesc.illas@ub.edu

Abstract

Recent experiments motivated by solar light harvesting applications have brought a renewed interest in $AgBiS_2$ as an environmentally friendly material with appealing photovoltaic properties. The lack of detailed knowledge on its bulk structural and electronic structure however inhibits further development of this material. Here we have investigated by first principles quantum mechanical methods models of the two most commonly reported $AgBiS_2$ crystal structures, the room temperature matildite structure, and the metastable schapbachite. Density functional theory (DFT) based calculations using the Perdew-Burke-Ernzerhof exchange-correlation (xc) functional reveal that matildite can be 0.37 eV per $AgBiS_2$ stoichiometry unit more stable than a schapbachite structure in bulk, and that the latter, in its ordered form, may display a metallic electronic structure, precluding its use for solar light harvesting. This points out the fact that $AgBiS_2$ nanocrystals used in solar cells should present a structure based on matildite. Matildite is found to be an indirect gap semiconductor, with an estimated bandgap of ~1.5 eV according to DFT based calculations using the more accurate hybrid xc functionals. These reveal that hole effective mass is twice that of electron effective mass, with concomitant consequences for the generated exciton. Hybrid DFT calculations also show that matildite has a high dielectric constant pertinent to that of an ionic semiconductor and slightly higher than that of PbS, a material that has been extensively used in solar cells in its nanocrystalline form. The calculated Bohr exciton radius of 4.6 nm and the estimated absorption coefficient of 10^5 cm^{-1} within the solar light spectrum are well in line with those experimentally reported in the literature.

I. Introduction

The mixed Silver-Bismuth sulphur ($AgBiS_2$) material has recently driven much attention in the scientific research community due to its use in the nanocrystalline form for high-performance solar cells [1]. Moreover, its ultralow thermal conductivity allows for its use in thermoelectric power generation [2,3], and it has also been explored as sensitizer and/or counter-electrode in sensitized solar cells [4,5]. The renewed interest on $AgBiS_2$ goes hand by hand with other compounds of the I-V-VI_2 family —where I = Cu, Ag, or an alkali metal; V = Sb or Bi, and VI = S, Se, or Te— studied in the recent times in thermoelectrics [2,6], solar cells [1,7], and phase-change memory devices [8,9].

Despite the above-commented unarguable interest, the amount of the so-far carried scientific research on $AgBiS_2$ is modest, and the lack of fundamental knowledge is evidenced by experimental observations that are at some point contradictory. For instance, the bandgap E_g, a fundamental property in semiconductors, was reported to be of solely 0.9 eV in $AgBiS_2$ bulk [10], yet more recent estimations report a value of 2.67 eV, although for quantum dots of 8.5 ± 1.2 nm [11], and of 2.78 eV for an average size of 7.6 nm [12]. These larger E_g values have been accounted for by strong quantum confinement effects. However, more recent experiments report a reduced value of 1.3 eV even for smaller nanoparticles of 4.62 ± 0.97 nm size [1]. Other bulk E_g measurements report a value 1.2 eV [5], which would limit the extend of quantum confinement effects; indeed some authors report E_g values of 1.32 eV for ~16 nm diameter samples [7], and values of 1.11 eV for $AgBiS_2$ thin films [13], in accordance to optical measurement of 1.10 eV [14].

The above discussion does not limit to E_g. For instance, a gigantic dielectric constant is claimed in previous studies on $AgBiS_2$ nanocrystallites [11], whereas orders of magnitude lower values were determined on other samples [1], although one has to regard the complexity, certain times uncertainty, in experimentally measuring dielectric constants. Even more, Ag rich samples are found in the literature [1], but, at the same time, Ag poor samples have been reported [11,15], together with estimates of much smaller Ag vacancy formation energies [16]. Last but not least, different synthesis methods lead to notoriously different nanoshapes, and these may have markedly different physicochemical properties [12,15,17]. The theoretical assessment of the electronic structure properties $AgBiS_2$ to date could be considered anecdotal, with, as

far as we know, a single recent study based on density functional theory (DFT) where high temperature disorder and native defect formation energies were tackled [16]. Apart from this initial study, the theoretical and computational study of $AgBiS_2$ is missing, and hence, this becomes a hindrance in the understanding of the properties of this material, the origin of the observed experimental discrepancies, and, ultimately, in the rationale of improving a particular property of interest. The present study aims at supplying a sound theoretical foundation by relying on a state-of-the-art DFT study of the known bulk crystallographic structures of $AgBiS_2$, including a study of stability aspects, as well a profound analysis of the electronic structure and derived optical properties.

II. Computational details

First, available experimental crystallographic structures of $AgBiS_2$ were acquired, including matildite (Pearson symbol *hP*12 and space group 164, *i.e.* $P\bar{3}m1$) and one schapbachite structure (Pearson symbol *cF*8 and space group 225, *i.e.* $Fm\bar{3}m$) [18,19]. Figure 1 depicts matildite rhombic unit cell contained within a larger cubic bulk unit cell, and one can simply think on it as a face-centred cubic arrangement of S atoms, in which Ag and Bi atoms insert in a NaCl fashion, being alternated in each of the three cell directions. In comparison, cubic unit cell of schapbachite is contained inside a larger bulk supercell of similar dimensions to that of matildite, and one can visualize it as a layered display of squared dispositions of AgS and BiS planes in a given cell direction.

Calculations have been carried out within the DFT framework using chiefly the Vienna *ab initio* simulation package VASP [20]. Most of the calculation rely on the use of the Perdew-Burke-Ernzerhof (PBE) exchange-correlation (xc) functional [21], a well-known member of the family of functionals issued from the generalized gradient approximation (GGA). Nevertheless, since GGA functionals are known to underestimate bandgaps of oxides and related systems, the PBE0 [22], B3LYP [23], and HSE06 [24] hybrid xc functionals, containing a fraction of non-local, exact, Fock exchange have also been used to explore the electronic structure of these materials. In particular, band structures have been obtained using the B3LYP functional and the CRYSTAL code [25]. In these calculations S was treated at the all electron level whereas a relativistic effective core potential has been used to describe the inner shells

of Ag and Bi. In all cases sufficiently large basis set of Gaussian Type Orbitals were used taken from the relevant literature [26-28].

In the calculations using a plane-wave basis, to represent the valence electronic density, a kinetic energy cutoff of 415 eV has been used and the effect of the core electrons in the valence electronic density was taken into account using the projected augmented-wave (PAW) method as implemented in VASP [29,30]. Note in passing by that the PAW method is effectively all electron with a frozen core including relativistic effects, especially important for heavy elements such as Ag or Bi. Whatever the computing package (VASP or CRYSTAL), a **k**-points Monkhorst-Pack [31] mesh of 9×9×3 dimensions was used for the rhombic unit cell of matildite and a mesh of 5×5×5 dimensions has been used for the cubic supercell. In the case of schapbachite, a **k**-points mesh of 9×9×9 has been used for the unit cell, and again a 5×5×5 mesh for the larger supercell depicted in Fig. 1. The used **k**-points and plane waves cutoff ensure a convergence in energy below 0.04 eV.

Atomic positions and cell dimensions were allowed to fully relax until forces acting on atoms were below 0.01 eV $Å^{-1}$. Calculations were carried in a spin-polarized fashion, although the total magnetic moments were found to be nominally zero, and so further analysis was carried out in a non spin-polarized manner. A tetrahedron method was used for the smearing, with an energy window of 0.1 eV, although final energies are extrapolated to 0 K.

Atomic charges have been estimated through a Bader analysis [32,33]. Simulated X-ray diffraction (XRD) patterns have been acquired employing the crystal prediction toolkit [34]. Band structures have been obtained by sampling 50 points along pre-defined vectors in the reciprocal space connecting high-symmetry points, see below. This sampling of the reciprocal space (density of **k**-points) has been found to be dense enough to capture band curvatures. The Bohr exciton radius, a parameter measuring electron/hole pair separation in quantum dots, r_B, can be determined from

$$r_B = \frac{\hbar^2 \varepsilon}{e^2}\left(\frac{1}{m_e} + \frac{1}{m_h}\right) \quad (1),$$

where $\hbar$ is the reduced Planck constant, e the charge of an electron, ε the dielectric constant, and m_e and m_h the electron and hole effective masses, respectively. The

effective masses are estimated, in a first approximation, assuming a parabolic dispersion of the conduction band (CB) maximum and valence band (VB) minimum, in the form:

$$E(\boldsymbol{k}) = \frac{\hbar^2|\boldsymbol{k}|^2}{2m} \quad (2)$$

where *E(**k**)* is the band energy at point **k** defined by the **k**-vector with module |**k**| and *m* is the effective mass. In this sense, the effective masses are obtained from the curvature of the band minima or maxima adjusted to a second degree polynomial, as done in previous work on ZnO [35], and values given in units of electron mass, m^*.

The frequency (ω) dependent complex dielectric constant ε is defined as

$$\varepsilon(\omega) = \varepsilon_r(\omega) + i\varepsilon_i(\omega) \quad (3),$$

where ε_r and ε_i are the real and imaginary parts [36]. The complex refractive index $N(\omega)$ is defined as [37,38]

$$N(\omega) = n(\omega) + ik(\omega) \quad (4),$$

where $n(\omega)$ and $k(\omega)$ can be related to $\varepsilon_r(\omega)$ and $\varepsilon_i(\omega)$ *via*

$$n(\omega) = \left(\frac{\sqrt{\varepsilon_r(\omega)^2+\varepsilon_i(\omega)^2}+\varepsilon_r(\omega)}{2}\right)^{\frac{1}{2}} \quad (5),$$

$$k(\omega) = \left(\frac{\sqrt{\varepsilon_r(\omega)^2+\varepsilon_i(\omega)^2}-\varepsilon_r(\omega)}{2}\right)^{\frac{1}{2}} \quad (6).$$

Then, the reflection coefficient $R(\omega)$ can be obtained from the normal electromagnetic incidence onto a plane surface as in Eq. 7,

$$R(\omega) = \frac{(n(\omega)-1)^2+k(\omega)^2}{(n(\omega)+1)^2+k(\omega)^2} \quad (7),$$

and further, the absorption coefficient $\alpha(\omega)$ can be evaluated from $k(\omega)$ as

$$\alpha(\omega) = \frac{2\omega k(\omega)}{c} \quad (8),$$

where *c* is the light speed in vacuum.

III. Results and discussion

The atomic structure of bulk matildite and schapbachite polymorphs of $AgBiS_2$ has been obtained from total energy minimization at the PBE level of theory. Lattice vectors, crystal cell angles, unit cell volume and density are listed in Table 1. It is to highlight the excellent agreement of DFT calculations in matching the experimental structures. The discrepancies on lattice parameters with respect experimental values are below 1% for matildite, and below 2% in schapbachite. However other properties, such as the volume *V*, and density, ρ, feature slightly larger discrepancies yet below 4%. In that sense one can claim that PBE is targeting the experimental structures, and actually these structures have been used in the forthcoming analysis. Note as well that other electronic structure based properties feature very slight variations when obtained on the experimental or the PBE optimized geometries, see below.

It is worth highlighting that present PBE total energies reveal matildite to be 0.37 eV per $AgBiS_2$ unit more stable than the simulated schapbachite, in perfect agreement with the reported value of 0.33 eV obtained at a similar computational level on the same models [16], implying that bulk schapbachite could be only found at high temperatures, in accordance to experimental observations at ~473 K [4,39]. Note, however, that, in those cases, a disordered structure is found where the two types of cations interchange in a rather random way. Other authors observe a similar disordered schapbachite *via* a thermopower change at ~610 K [16]. In this study, the modelled schapbachite structure possesses a predefined cation ordering considered as an $Fm\bar{3}m$ case in which AgS and BiS square parallel planes alternate perpendicular to a [001] crystal direction. On the contrary, in matildite, Ag atoms arrange in a rhombic pattern along (111) plane, for more details see Figure 1.

The different chemical environment in the two structures implies different structural features and electronic properties as well. For instance, in matildite the average *d*(Ag-S) and *d*(Bi-S) bond lengths are 2.73 and 2.89 Å, respectively. However, in schapbachite these are 2.86 and 2.77 Å respectively, implying a longer Ag-S bond, and, consequently, a shorter Bi-S bond. However, the average cation-anion bond distance in both cases is ~2.82 Å, thus equidistant from the experimental mean value of 2.87 Å reported in the literature [1].

When it comes to the oxidation state, the differences between both polymorphs are minimal, with variations of Bader charges below 0.2 *e*, see Table 2. Note here that $AgBiS_2$ can be considered a highly ionic material. However, Bader charges usually differ from those corresponding to formal oxidations states. Hence, from this single parameter it is difficult to assess the degree of ionicity of these materials. All that said, the ionic character seems to be a main ruler, as the proportion of charges is well kept among the elementary constituents. It is worth to mention that Bader charges obtained using the experimental structure feature no significant changes with respect to those corresponding to the optimized one. Also, only small variations below 0.18 *e* are found when acquiring Bader charges from single point electronic densities obtained at PBE0 or HSE06 xc levels, and so, ionicity seems to be well described at any of the computed levels.

Regarding XRD patterns, simulations by using a Co-based X-ray target for both matildite and schapbachite are shown in Figure 2, displaying that, in both periodic structures, different diffraction peaks at different 2Θ angles with different intensities exist, yet some signatures would interfere with others. However, focusing on the dominant signals and their intensities one can conclude that present results for matildite structure are much closer to the $AgBiS_2$ XRD patterns reported in the literature [1,15,40]. However the fitting is not fully perfect, and actually it may well be that native defects and/or a certain degree of disorder affects the experimental XRD patterns.

The most important difference between matildite and schapbachite $AgBiS_2$ crystalline structures sits on their electronic structure. Figure 3 shows the explored lines connecting high symmetry **k**-points in their respective reciprocal space Brillouin zones, accompanied with the plotted dispersion of the valence and conduction bands near the Fermi level, E_F. Figure 3 shows that whereas matildite is a narrow gap semiconductor, the schapbachite structure has a metallic character with a clear zero bandgap E_g. This feature alone would discard it for optoelectronic or solar harnessing applications, given the excited electron relaxation channels found near **R**, **M**, and **A** **k**-points. This does not happen in matildite, where a bandgap region is found for all **k**-space explored points in between valence band maximum (VBM) and conduction band minimum (CBM). According to present results, bulk matildite $AgBiS_2$ is a narrow indirect gap semiconductor with a VBM located along the **K→Γ** line, whereas CBM is located at the **A** high symmetry point.

It is worth pointing out that the magnitude of the band gap predicted by the DFT based calculations within the PBE functional (0.42 eV) is markedly smaller than the above-commented measurements. However, PBE and other DFT xc functionals of the GGA family are long known to heavily underestimate bandgaps in semiconductors and insulators, stemming out from DFT intrinsic electronic self-interaction error. As noted initially by Muscat *et al.* from periodic calculations with the hybrid B3LYP functional [41], and confirmed by several authors on a variety of different insulators [42-44], a more accurate prediction of the magnitude of the bad gap in this type of highly ionic insulators requires the use of hybrid xc functionals.

Table 3 contains the single-point estimates of E_g as obtained using PBE0, HSE06, or B3LYP hybrid xc functionals on top of the PBE optimized geometries. Tests on matildite experimental geometry yielded variations of E_g of 0.19 eV in average, where B3LYP features the smaller discrepancy, of solely 0.01 eV. The hybrid xc functional estimates, ranging 1.5-1.9 eV, are much more reliable and in line with experimental measurements of 0.9-1.2 eV [5,10]. Present results suggest to use a reduced percentage of Fock exchange of 8 to 13% to target an assumed experimental E_g value of 0.9 to 1.2 eV. This is in line with recent work for TiO_2 where the band gap of rutile and anatase is properly reproduced when the xc functional contains a 12.5% of Fock exchange [45], which is half of the standard value in PBE0 and HSE06.

Table 3 shows that E_g vales are clearly underestimated when Fock exchange is lacking, as in PBE. By adding a 25% of Fock exchange the bandgap is increased to 1.88 eV, and one could argue that this is even too much since at the PBE0 level schapbachite features a small but noticeable bandgap of 0.53 eV. This overestimation tends to be counteracted by the screening factor applied in range-separated HSE06 functional, which features a smaller bandgap of 1.54 eV for matildite. At this level, the obtained separation of VBM and CBM in schapbachite is of 0.09 eV only and hence, within the limits of DFT accuracy, it could be considered back as metallic. The screening parameter applied in HSE06 seems to be equivalent to the reduced 20% Fock exchange in B3LYP, with a very similar bandgap of 1.57 eV. These differences are also observed when plotting the atomic decomposed density of states (DOS), as depicted in Figure 4. Notice here how, for matildite, at any DFT xc level, the VBM and nearby states are clearly dominated by the S 3*p* orbital derived levels, whereas CBM and close bands are mostly governed by Bi. This extends as well to schapbachite, although here Ag related

states play a more determining role near the Fermi level, and because of this, one could argue that AgS planes, as shown in Figure 1, are likely to be the origin of the $AgBiS_2$ schapbachite model metal character.

At this point we further focus on matildite $AgBiS_2$ as being the crystallographic arrangement with potential for optoelectronic and solar cell applications. One aspect worth to investigate is to determine the electron/hole effective masses, which would deliver hints on the possible lattice movement of the exciton components. Indeed, a larger difference among masses would intuitively suggest that such charge carriers separate more efficiently, and so, they would be more unlikely to recombine and lead the system to its electronic ground state. In accordance, a larger Bohr exciton radius would be obtained, following Eq. (1), considered as a mean separation between the excited electron and the created hole.

Effective masses have been estimated on the VBM and CBM, as above commented and shown in Figure 3, although at B3LYP level. Notice that the electron self-interaction error present in PBE not only reduces the E_g, but also sharpens band curvatures, which would be eventually translated into artificially lighter effective masses. The B3LYP band structure, as well as the others obtained with other hybrid xc functionals, feature the same band structure, with only variations in E_g and band dispersions. Accordingly, present results based on B3LYP band structure reveal an effective hole mass m_h of 0.722 m^* at the VBM located along the **K**→**Γ** line, whereas the excited electron displays an effective mass m_e of 0.350 m^* obtained at **A** along **H** direction. Note that effective masses evaluation has been restricted to *a* and *b* equivalent matildite crystallographic directions, disregarding *c* direction, which features lower curvatures and so, assumedly, larger effective masses. Thus, focussing on main charge mobility directions, apparently the fact that the hole effective mass doubles that of the excited electron can be interpreted as facilitating a large separation of the electron/hole pair along *ab* planes, with a concomitant sufficient large time survival of the exciton.

Another property to be considered is the frequency dependent dielectric function. The imaginary part of the dielectric function, $\varepsilon_i(\omega)$, is intimately related to the frequency-dependent optical response. Figure 5 shows a band split-off at lower energies at PBE level, but at larger energies at HSE06 and PBE0, in concordance with E_g values shown in Table 3. A striking feature is that the highest peak, as obtained at any DFT xc

functional level, has intensity values in the 30-60 range. This is 3-5 times higher than the values obtained for bulk TiO_2 anatase, brookite, and rutile [46], an extendedly known photoactive material used in photocatalysis. This feature would align with previous statements of an anomalously large dielectric constant [11]. Note that regarding the previous TiO_2 work, a slightly different computational method was used, the so-called Hubbard U correction (PBE+U) by Dudarev *et al.* [47]. Consequently, a direct comparison is not advised, although little variations are expected; at least, lesser than when comparing PBE to hybrid functionals PBE0 or HSE06. Aside from this, there is little variation in between the orthogonal dielectric function component, $\varepsilon_{\perp}$, corresponding to *a* and *b* cell vector directions, and the parallel component, $\varepsilon_{\parallel}$, corresponding to the *c* cell vector direction. According to this, $AgBiS_2$ seems to not feature anisotropy in light absorbance.

The static macroscopic dielectric constant, ε, has been estimated in two ways; either through the evaluation of the piezoelectric tensor, or as the value of the frequency dependent real part of the dielectric function at $\omega = 0$, here called ε^{apx}. For details of the procedure we refer to the specialized literature [48]. Both quantities have been gained at PBE, PBE0, and HSE06 levels. Moreover, a comparison has been made between matildite $AgBiS_2$ and other semiconductors broadly studied in the literature, which encompass cubic diamond (C), silicon (Si), silicon carbide (SiC), and gallium arsenide (GaAs). Since these materials were studied using the Ceperley-Alder (CA) xc functional [49] based on the so-called local density approximation (LDA), the value for $AgBiS_2$ have also been acquired at this level of theory, thus providing a fair comparison. To complete the picture, we studied as well a wide bandgap inert oxide, MgO, and another chalcogenide, PbS, considered as a candidate for solar cells [50]. These have been optimized self-consistently at CA and PBE levels. All estimated values are compared to experimental reported values [51-53].

In light of the dielectric constant values, shown in Table 4, several conclusions can be withdrawn. On one hand, ε and ε^{apx} values are very similar, with discrepancies in the worst case ($AgBiS_2$) below 6%, and in some cases (SiC) providing exactly the same quantity. Aside, CA estimates seem to be closer to experiments than PBE ones. Actually, by inspecting ε^{apx} data one observes that the use of hybrid functionals seem to be detrimental for dielectric constants, despite its benefits in estimating band gaps. In

accordance to other computed semiconductors and insulators, and their experimental values, it seems that for this observable parameter the CA estimates are more reliable. Accordingly, one can safely conclude that bulk matildite $AgBiS_2$ would have a dielectric constant just marginally larger than that of PbS. Indeed, this finding supports the observed photoactivity of $AgBiS_2$, and, in addition, suggests that the reported dielectric constants in $AgBiS_2$ pellets [11], orders of magnitude higher, are likely due to surface dipole effects instead of bulk related properties.

By considering the most reliable simulated values for ε obtained at CA level, and the m_h and m_e effective masses obtained at B3LYP level, one can grossly estimate a Bohr exciton radius of 4.6 nm, which coincides with the reported nanoparticle mean size in the previous experimental study on their use on solar cell devices [1], and would preclude invoking quantum size effects on larger nanoparticles [11,12], suggesting stoichiometry variation or surface effects as the origin of bandgap variability.

Last but not least, absorbance spectra have been acquired using hybrid functionals. For technical reasons, the PBE0 and HSE06 functionals have been employed (Figure 6). Here it is worth to point out that o estimate the band gap from the electronic structure is a well established procedure and the one followed here. Using the thus computed band gap one can also determine the onset for absorption which is used in experiment to gain this property and not always uniquely determined. With this in mind, the similarity of results for the two hybrid functionals is remarkable and consistent with highly similar values of the dielectric constant reported in Table 4. These employed DFT based methods capture the absorbance intensity reported in the literature of 10^5 cm^{-1} [1]. However the slow decay by increasing the radiation wavelength is better captured by using hybrid functionals. Likewise, the abrupt decay in Figure 6 at ~1500 nm is similar to what is found experimentally, although red-shifted by 400 nm. The origin of the shift can be attributed to limitations of the theoretical approach and/or to deviations of the electronic structure of the nanoparticles from the perfect arrangement of the bulk. In fact, note that other nanocrystals samples imply a much more earlier decay of at around 400 nm [11,40]. In any case, present theoretical results show that, as far as bulk matildite is concerned, absorbance would not deviate from 10^5 cm^{-1} in the 400-700 nm visible light region, thus supporting solar light harvesting applications. As above commented a variety of factors, here not contemplated, such as nanoparticle shape (biased by the preparation method), non-

stoichiometry composition, boundary region effects, and/or presence of bulk defects or certain degrees of cationic disorder may be determinant factors which influence the absorbance spectrum.

IV. Conclusions

Motivated by the renewed interest in $AgBiS_2$ for solar light harvesting applications, and by the lack of detailed knowledge on its bulk structural and electronic structure, we have studied this material using first principles quantum mechanical methods considering two reported crystal structures, the room temperature matildite structure, and a metastable ordered schapbachite arrangement. DFT based for the bulk structures carried out at the PBE level show that matildite can be 0.37 eV per $AgBiS_2$ stoichiometry unit more stable than the schapbachite arrangement, and that the latter displays a metallic character in its electronic structure, *i.e.* no bandgap.

Metal-sulfur interatomic distances are in line with those experimentally observed in employed nanocrystals, and a high degree of ionicity is present in matildite, according to Bader charges. Matildite is found to be an indirect gap semiconductor, with an estimated bandgap of ~1.5 eV according to DFT calculations using state of the art HSE06 and B3LYP hybrid density functionals. The B3LYP estimated VBM m_h effective mass doubles that of CBM m_e, suggesting a longer survival of a generated exciton. Estimates of the matildite $AgBiS_2$ dielectric constant reveal that is slightly higher than that of PbS, another material considered in solar cells. The here calculated Bohr exciton radius is 4.6 nm, thus similar to nanocrystals sizes found in the literature, and the experimentally absorbance intensities of 10^5 cm^{-1} in the solar light absorbance region are well reproduced according to present calculations.

Acknowledgements: This work has been supported by Spanish Ministry of Economy and Competitiveness (MINECO) and *Fondo Europeo de Desarrollo Regional* (FEDER) CTQ2015-64618-R and MAT2014-56210-R grants and partly by *Generalitat de Catalunya* grants 2014SGR97, 2014SGR1548, and XRQTC, the *Fundación Privada Cellex*, and the European Community Seventh Framework Programme (FP7-ENERGY.2012.10.2.1) under agreement N^o 308997. The research in this work is in the framework of the NOMAD Center of Excellence project which received funding from

the European Union's Horizon 2020 research and innovation programme under grant agreement N^{o} 676580. F.V. thanks MINECO for a postdoctoral *Ramón y Cajal* (RyC) research contract (RYC-2012-10129). F.I. acknowledges additional support from the 2015 ICREA Academia Award for Excellence in University Research. G.K. acknowledges financial support from the Spanish Ministry of Economy and Competitiveness, through the *Severo Ochoa* Programme for Centres of Excellence in R&D (SEV-2015-0522).

Figure 1. Matildite (left) either in the rhombic unit cell (orange lines, bold spheres) or in the cubic supercell (black lines, glass small spheres), and schapbachite (right) either in the cubic unit cell (orange lines, bold spheres) or in the cubic supercell (black lines, glass small spheres). Grey, pink, and yellow spheres denote Ag, Bi, and S atoms, respectively.

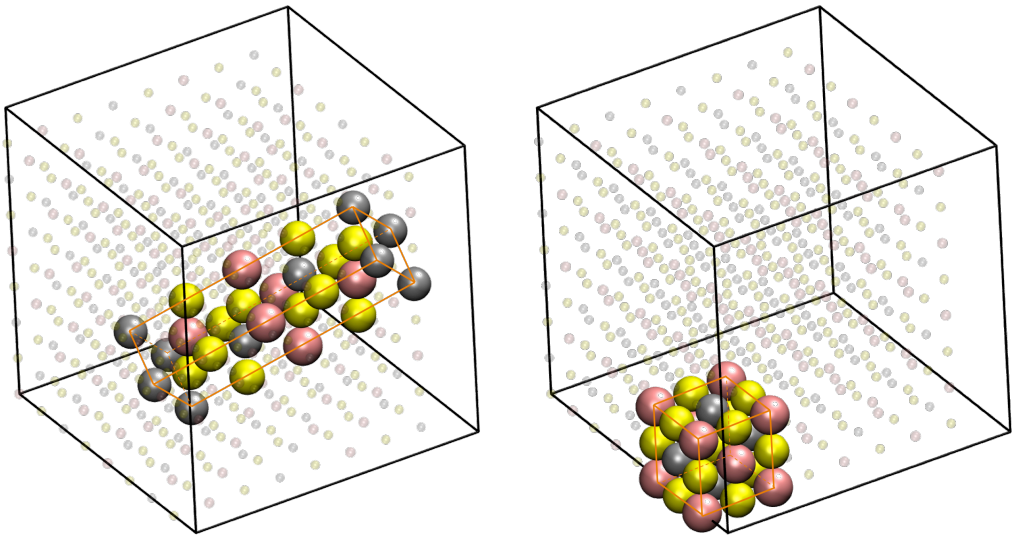

Figure 2. Simulated XRD pattern, showing intensity *versus* 2Θ angle, for matildite (top) and schapbachite (bottom).

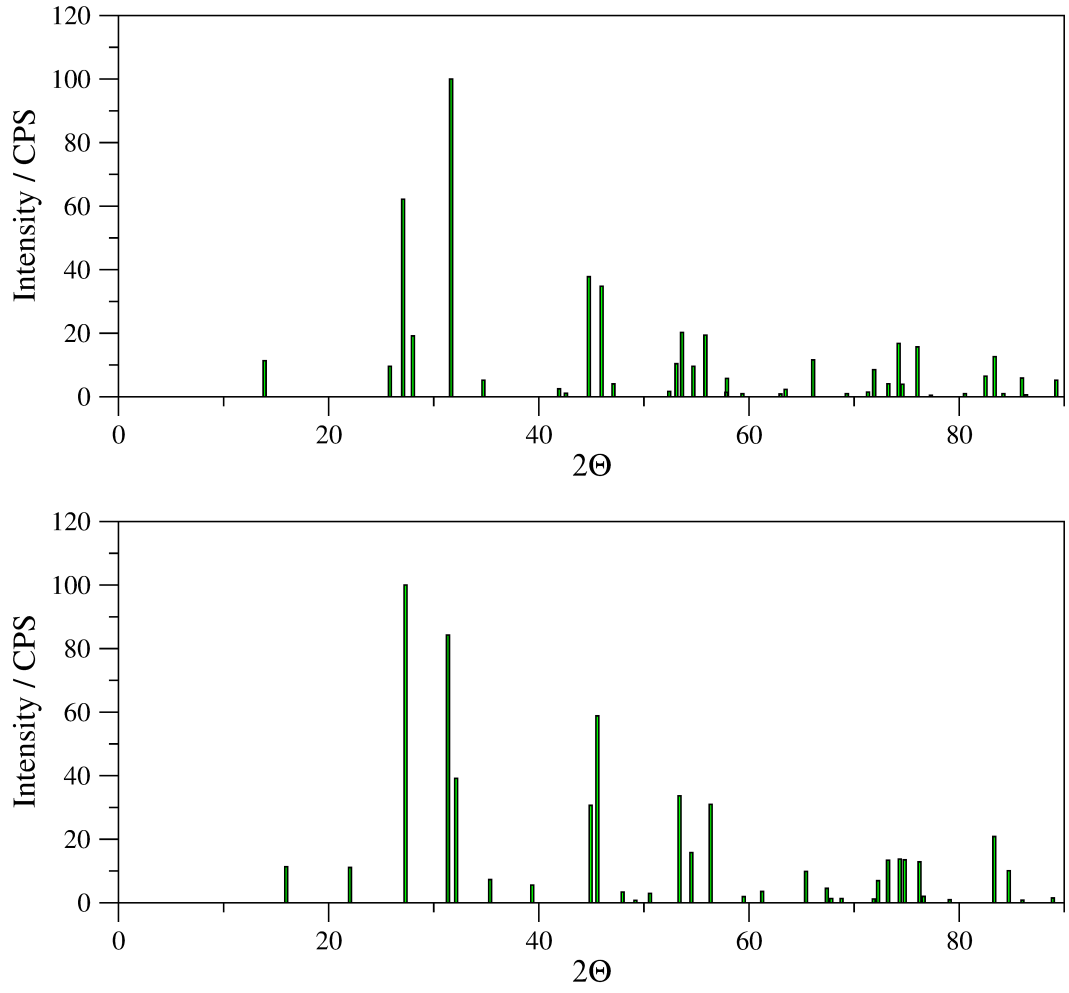

Figure 3. Brillouin zones (top) of unit cells of matildite (left) and schapbachite (right) $AgBiS_2$. Reciprocal lattice vectors are shown as red lines. High symmetry lattice points are named, and connected trough green lines. The bandstructure of both crystals are shown (bottom) as obtained at the PBE xc level, with band energies scaled to Fermi level, E_F. High symmetry **k**-points are noted, as well as the gap region in between VBM and CBM, colored yellow.

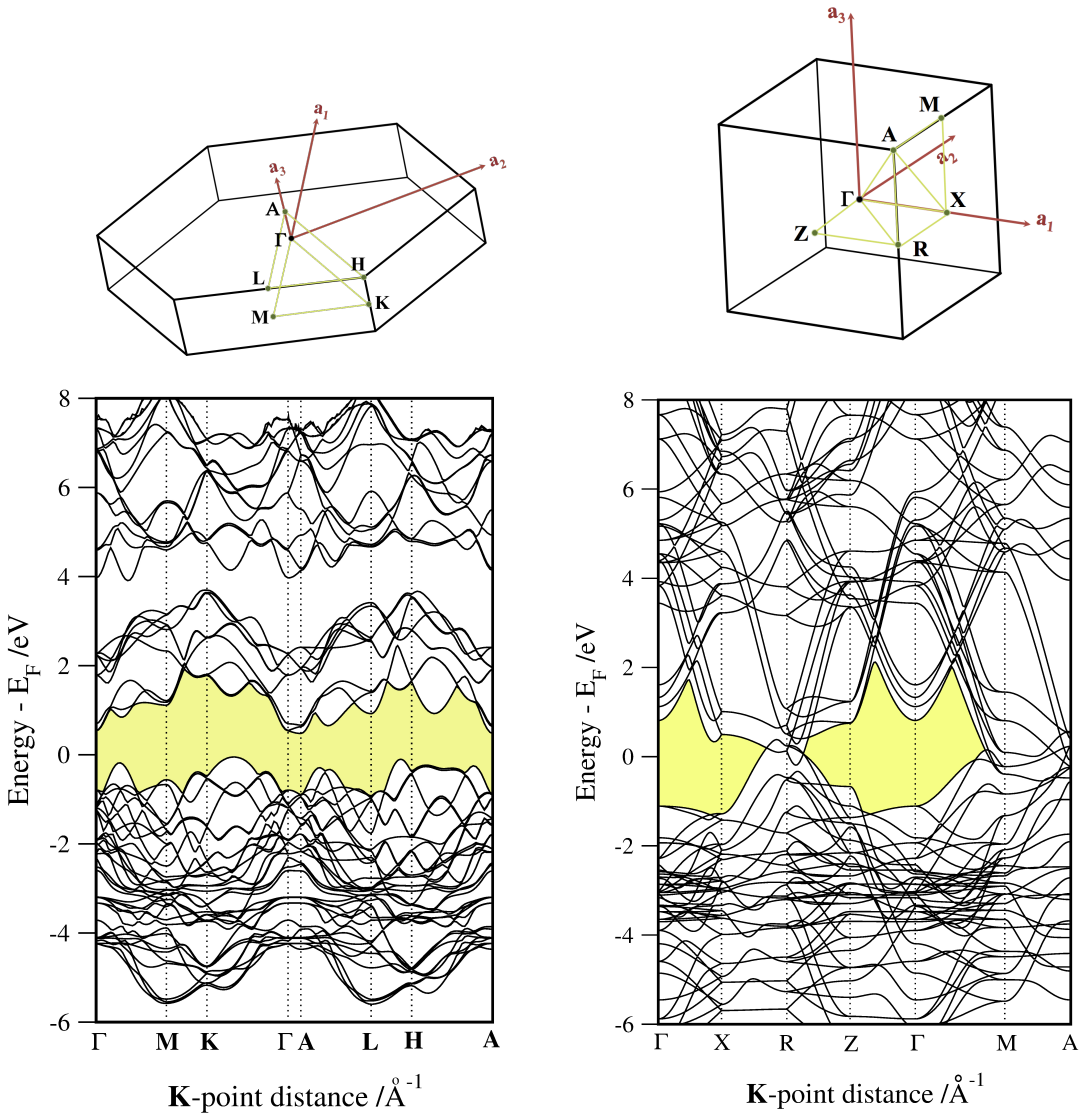

Figure 4. Atomic projected density of states (DOS) for matildite (left) and schapbachite (right) bulk $AgBiS_2$ structures at the PBE, HSE06 and PBE0 corresponding to the PBE optimized crystal structure. Total DOS is shown black, and atom contributions color-coded as in Fig. 1.

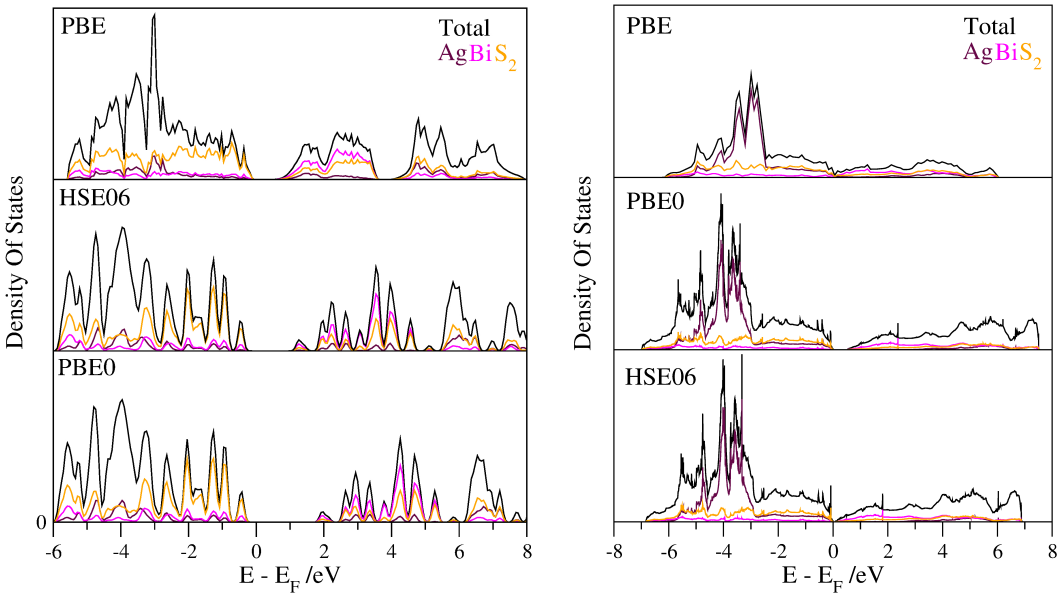

Figure 5. Frequency (ω) dependent average imaginary part of the dielectric function, here $\bar{\varepsilon}(\omega)$. Total averaged value is shown as a black line, but orthogonal, $\varepsilon_{\perp}$, and parallel, $\varepsilon_{\parallel}$, contributions are shown in red and blue lines, respectively.

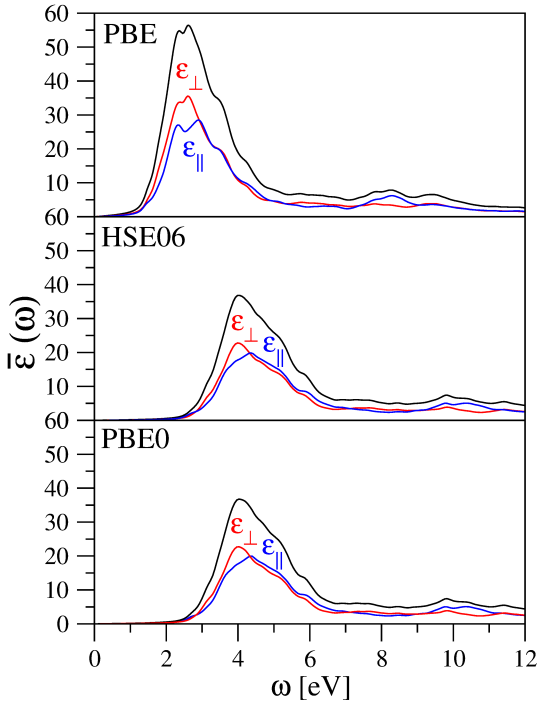

Figure 6. Absorption coefficients, α, in cm^{-1}, with respect different wavelengths, in nm, estimated at PBE0 and HSE06 levels.

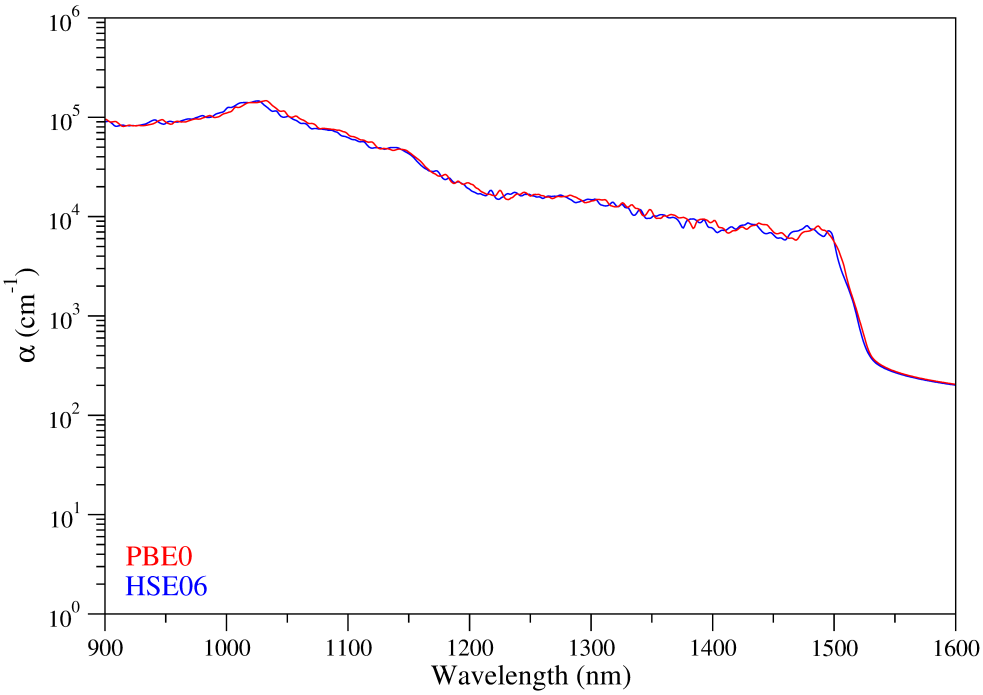

Table 1. Experimental (Exp.) and calculated (PBE) matildite and schapbachite $AgBiS_2$ crystal structures, encompassing unit cell dimensions, *a* and *c*, their ratio *c*/*a*, their lattice vector angle, α and γ, respectively, their volume, *V*, and the associated density ρ, as well as the reported or PBE computed bandgap E_g.

	Maltidite		**Schapbachite**	
Parameter	**Exp.**[a]	**PBE**	**Exp.**[b]	**PBE**
***a* / Å**	4.0662	4.0497	5.648	5.723
***c* / Å**	18.958	19.109	—	—
α / °	90	90	90	90
γ / °	120	120	—	—
c*/*a	4.662	4.699	—	—
***V* / Å^3**	271.46	271.41	180.17	187.41
ρ / g·cm^{-3}	7.57	7.58	4.23	4.07
***E*$_g$ / eV**	0.9	0.42	—	0.0

[a] Ref. [10,18], [b] Ref. [19].

Table 2. Formal and Bader charges for atoms in bulk $AgBiS_2$. The Bader charges are derived from the PBE calculations on the optimized matildite (mat.) and schapbachite (sch.) structures.

Atom	Ideal	Mat.	Sch.
Ag	+1	+0.47	+0.39
Bi	+3	+1.21	+1.41
S	-2	-0.83	-0.90

Table 3. Calculated band gaps, E_g, in eV, for matildite and schapbachite bulk $AgBiS_2$, as obtained by single-point calculations at PBE, PBE0, HSE06, and B3LYP exchange correlations functionals on previously optimized bulk geometries gained at PBE level.

E_g	Mat.	Sch.
PBE	0.42	0.00
PBE0	1.88	0.53
HSE06	1.54	0.09
B3LYP	1.57	—

Table 4. Static macroscopic dielectric constants, ε, and approximated static macroscopic dielectric constants, ε^{apx}, calculated for a series of semiconductor and insulator materials, using different xc functionals. Experimental values are shown when possible.

		$AgBiS_2$	C	Si	SiC	GaAs	MgO	PbS
ε	**CA**	19.29	5.98[a]	14.08[a]	7.29[a]	14.77[a]	3.09	20.36
	PBE	17.29	—	—	—	—	3.11	15.59
	HSE06	—	—	—	—	—	—	—
	PBE0	—	—	—	—	—	—	—
ε^{apx}	**CA**	20.44	5.98[a]	14.04[a]	7.29[a]	14.75[a]	3.19	19.99
	PBE	18.21	—	—	—	—	3.15	15.45
	HSE06	9.67	—	—	—	—	—	—
	PBE0	9.68	—	—	—	—	—	—
	Exp.	—	5.70[b]	11.90[b]	6.52[b]	11.10[b]	2.96[c]	17.20[d]

[a] Ref. [48], [b] Ref. [51], [c] Ref. [52], [d] Ref. [53].

References:

[1] M. Bernechea, N. C. Miller, G. Xercavins, D. So, A. Stavrinadis, and G. Konstantatos, Nat. Photon. **10**, 521 (2016).

[2] S.N. Guin, A. Chatterjee, D.S. Negi, R. Datta, and K. Biswas, Energy Environ. Sci. **6**, 2603 (2013).

[3] C. Xiao, X. Qin, J. Zhang, R. An, J. Xu, K. Li, B. Cao, J. Yang, B. Ye, and Y. Xie, J. Am. Chem. Soc. **134**, 18460 (2012).

[4] S.N. Guin and K. Biswas, Chem. Mater. **25**, 3225 (2013).

[5] B. Pejova, D. Nesheva, Z. Aneva, and A. Petrova, J. Phys. Chem. C **115**, 37 (2011).

[6] S.N. Guin, V. Srihari, and K. Biswas, J. Mater. Chem. A **3**, 648 (2015).

[7] P.-C. Huang, W.-C. Yang, and M.-W. Lee, J. Phys. Chem. C **117**, 18308 (2013).

[8] J. Ma, O. Delaire, A.F. May, C.E. Carlton, M.A. McGuire, L.H. VanBebber, D.L. Abernathy, G. Ehlers, T. Hong, A. Huq, W. Tian, V.M. Keppens, Y. Shao-Horn, and B.C. Sales, Nat. Nanotechnol. **8**, 445 (2013).

[9] W. Welnic and M. Wuttig, Mater. Today **11**, 20 (2008).

[10] I.I. Golovach, N.I. Dovgoshei, V.Y. Slivka, L.M. Suslikov, M.I. Golovei, and A.V. Bogdanova, Izv. Vyssh. Uchebn. Zaved. Fiz. **3**, 39 (1976).

[11] C. Chen, X. Qiu, S. Ji, C. Jia, and C. Ye, CrystEngComm **15**, 7644 (2013).

[12] N. Liang, W. Chen, F. Dai, X. Wu, W. Zhang, Z. Li, J. Shen, S. Huang, Q. He, J. Zai, N. Fang, and X. Qian, CrystEngComm **17**, 1902 (2015).

[13] D. Nesheva, Z. Aneva, B. Pejova, I. Grozdanov, and A. Petrova, J. Optoelectron. Adv. M. **11**, 1347 (2009).

[14] B. Pejova, I. Grozdanov, D. Nesheva, and A. Petrova, Chem. Mater. **20**, 2551 (2008)

[15] M. Nakamura, H. Nakamura, T. Ohsawa, M. Imura, K. Shimamura, and N. Ohashi, J. Cryst. Growth **411**, 1 (2015).

[16] S.N. Guin, S. Banerjee, D. Sanyal, S.K. Pati, and K. Biswas, Inorg. Chem. **55**, 6323 (2016).

[17] J. Yan, J. Yu, W. Zhang, Y. Li, X. Yang, A. Li, X. Yang, W. Wang, and J. Wang, J. Mater. Sci. **47**, 4159 (2012).

[18] P. Bayliss, Amer. Mineral. **76**, 1991, 257-265.

[19] A.C. Glatz and A. Pinella. J. Mater. Sci. **3**, 1968, 498-501.

[20] G. Kresse and J. Furthmüller, Phys. Rev. B **54**, 11169 (1996).

[21] J.P. Perdew, K. Burke, and M. Ernzerhof, Phys. Rev. Lett. **77**, 3865 (1996).

[22] C. Adamo and V. Barone, J. Chem. Phys. **110**, 6158 (1999).

[23] A.D. Becke, J. Chem. Phys. **98**, 5648 (1993).

[24] J. Heyd, G.E. Scuseria, and M. Ernzerhof, J. Chem. Phys. **118**, 8207 (2003).

[25] R. Dovesi, R. Orlando, A. Erba, C.M. Zicovich-Wilson, B. Civarelli, S. Casassa, L. Maschio, M. Ferrabone, M. de la Pierre, P. d'Arco, Y. Noel, M. Causa, M. Rerat, and B. Kirtman, Int. J. Quantum Chem. **114**, 1287 (2014).

[26] K. Doll, P. Pykkö, and H. Stoll, J. Chem. Phys. **109**, 2339 (1998).

[27] R. Weihrich and I. Anusca, Z. Anorg. Allg. Chem. **632**, 335 (2006).

[28] M.F. Peintinger, D. Vilela-Oliveira, and T. Bredow, J. Comput. Chem. **34**, 451 (2012).

[29] P. E. Blöchl, Phys. Rev. B **50**, 17953 (1994).

[30] G. Kresse, D. Joubert, Phys. Rev.B **59**, 1758 (1999).

[31] H.J. Monkhorst and J.D. Pack, Phys. Rev. B **13**, 5188 (1976).

[32] G. Henkelman, A. Arnaldsson, and H. Jónsson, Comput. Mater. Sci. **36**, 254 (2006).

[33] R.F. Bader, *Atoms in Molecules: A Quantum Theory,* Oxford Science, Oxford, UK, 1990.

[34] G. Hautier, V. Ehrlacher, C.C. Fischer, A. Jain, and G. Ceder, Inorg. Chem. **50**, 656, 2011.

[35] A. Iglesias-Juez, F. Viñes, O. Lamiel-García, M. Fernández-García, and F. Illas, J. Mater. Chem. A **3**, 8782 (2015).

[36] F. Wooten, *Optical Properties of Solids*, Academic Press, 2013.

[37] A.M. Fox, *Optical Properties of Solids*, Vol. 3, Oxford University Press, USA, 2001, 045112.

[38] M. Dressel and G. Grüner, *Electrodynamics of Solids: Optical Properties of Electrons in Matter*, Cambridge University Press, 2002.

[39] S. Geller and J.H. Wernick, Acta Crystallogr. **12**, 46 (1959).

[40] G. Shen, D. Chen, K. Tang, and Y. Qian, J. Cryst. Growth **252**, 199 (2003).

[41] J. Muscat, A. Wander, and N. M. Harrison, Chem. Phys. Lett. **342**, 397 (2001).

[42] I. de P. R. Moreira, F. Illas and R. L. Martin, Phys. Rev. B **65**, 155102 (2002).

[43] E. Finazzi, C. Di Valentin, G. Pacchioni and A. Selloni, J. Chem. Phys **129**, 154113 (2008).

[44] A. Janotti, J. B. Varley, P. Rinke, N. Umezawa, G. Kresse and C. G. Van de Walle, Phys. Rev. B **81**, 085212 (2010).

[45] K. C. Ko, O. Lamiel-García, J. Y. Lee, and F. Illas, Phys. Chem. Chem. Phys. **18**, 12357 (2016).

[46] S. Tosoni, D. Fernández-Hevia, O. González-Díaz, and F. Illas, J. Phys. Chem. Lett. **3**, 2269 (2012).

[47] S.L. Dudarev, G.A. Botton, S.Y. Savrasov, C.J. Humphreys, and A.P. Sutton, Phys. Rev. B: Condens. Matter Mater. Phys. **57**, 1505 (1998).

[48] M. Gajdoš, K. Hummer, G. Kresse, J. Furthmüller, and F. Bechstedt, Phys. Rev. B **73**, 045112 (2006).

[49] D.M. Ceperley and B.J. Alder, Phys. Rev. Lett. **45**, 566 (1980).

[50] C.M. Chuang, P.R. Brown, V. Bulovič, and M.G. Bawendi, Nat. Mater. **13**, 796 (2014).

[51] P.Y. Yu and M. Cardona, *Fundamentals of Semiconductors*, Springer-Verlag, Berlin, 2001.

[52] D.R. Lide, *CRC Handbook of Chemistry and Physics*, CRC Press/Taylor & Francis, Boca Ratón, Florida, 2010.

[53] N.M. Ravindra and V.K. Srivastava, Phys. Status Solidi A **58**, 311 (1980).